Langmuir

Article

pubs.acs.org/Langmuir

Distinctive Interactions of Oleic Acid Covered Magnetic Nanoparticles with Saturated and Unsaturated Phospholipids in Langmuir Monolayers

Thabo J. Matshaya,[§] Anabel E. Lanterna,[†] Alejandro M. Granados,[†] Rui W. M. Krause,[§] Bruno Maggio,[‡] and Raquel V. Vico*[,†]

[†]Instituto de Investigaciones en Fisicoquímica de Córdoba (INFIQC), CONICET and Departamento de Química Orgánica, Facultad de Ciencias Químicas, Universidad Nacional de Córdoba, Haya de la Torre y Medina Allende, Ciudad Universitaria, X5000HUA Córdoba, Argentina

[‡]Centro de Investigaciones en Química Biológica de Córdoba (CIQUIBIC), CONICET and Departamento de Química Biológica, Facultad de Ciencias Químicas, Universidad Nacional de Córdoba Haya de la Torre y Medina Allende, Ciudad Universitaria, X5000HUA Córdoba, Argentina

[§]Department of Chemistry, Rhodes University, PO Box 94, Grahamstown 6140, South Africa

Supporting Information

ABSTRACT: The growing number of innovations in nanomedicine and nanobiotechnology are posing new challenges in understanding the full spectrum of interactions between nanomateriales and biomolecules at nano-biointerfaces. Although considerable achievements have been accomplished by in vivo applications, many issues regarding the molecular nature of these interactions are far from being well-understood. In this work, we evaluate the interaction of hydrophobic magnetic nanoparticles (MNP) covered with a single layer of oleic acid with saturated and unsaturated phospholipids found in biomembranes through the use of Langmuir monolayers. We find distinctive interactions among the MNP with saturated and unsaturated phospholipids that are reflected by both, the compression isotherms and the surface topography of the films. The interaction between MNP and saturated lipids causes a noticeable reduction of the mean molecular area in the interfacial plane, while the interaction with unsaturated lipids promotes area expansion compared to the ideally mixed films. Moreover, when liquid expanded and liquid condensed phases of the phospholipid(s) coexist, the MNP preferably partition to the liquid-expanded phase, thus hindering the coalescence of the condensed domains with increasing surface pressure. In consequence organizational information on long-range order is attained. These results evidence the existence of a sensitive composition-dependent surface regulation given by phospholipid−nanoparticle interactions which enhance the biophysical relevance of understanding nanoparticle surface functionalization in relation to its interactions in biointerfaces constituted by defined types of biomolecules.

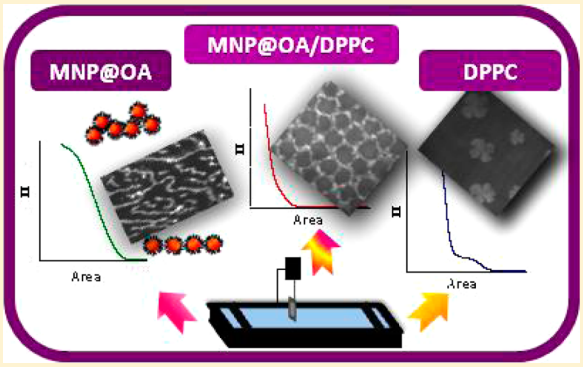

INTRODUCTION

Although a growing number of innovations have emerged in the fields of nanobiotechnology and nanomedicine, new engineered nanomaterials (ENMs) with novel physicochemical properties are posing new challenges in understanding the full spectrum of interactions at the nano−bio interface.[1,2]

An important topic in nanociences is to have the capacity to control at the molecular level the design of an interface of interpenetrating two-phased systems, where the surface morphologies and lateral organization are purposely tailored so as to be able to manipulate and functionalize them with features that can extend to the construction of self-assembled two- and three-dimensional nano- or microfluidic devices in relatively simple manner.[3]

Rapid growth in nanotechnology is increasing the likelihood of nanomaterials coming into contact with humans and the environment. Nanoparticles interacting with biological membranes establish a series of nanoparticle/biointerface effects that depend on colloidal forces as well as on dynamic biophysical factors.[4] Either for their defined molecular design and/or for biomedical applications, an increased understanding of the interactions between nanoparticles with biomolecules, biomembrane surfaces, cells, and whole organisms is increasingly required.[5,6] Nanoparticle charge, shape, as well as their shape anisotropy (or isotropy) play a critical role in the translocation

Received: March 7, 2014
Revised: April 25, 2014

   dx.doi.org/10.1021/la500903m | *Langmuir* XXXX, XXX, XXX−XXX

process through cell membranes.[7,8] It was demonstrated by using molecular dynamics simulation techniques that translocation rate constants of nanoparticles in model bilayers can vary greatly by modifying the factors above mentionated.[7] Particle membrane wrapping and particle adhesion to the lipid−protein bilayer at the cell surface is a prime example of an interface between nanomaterials and biomolecules that can be used for understanding the parameters involved in the molecular control of nanoparticle targeting, surface recognition, or molecular design for therapeutic use among others.

Magnetic nanoparticles (MNP) are greatly promising because of their potential application in fields such us drug delivery, magnetic resonance imaging (MRI) for contrast enhancement, stem cell tracking, and heat source in magnetic fluid hyperthermia.[5] Also, in biotechnology and biomedicine, magnetic separation can be used as a quick and simple method for the efficient and reliable capture/relase/removal of specific bioactive compounds and other biomolecules.[9] Although considerable achievements have been accomplished by in vivo applications,[10] many fundamental issues regarding the understanding of the molecular nature of the interactions between MNP with biomolecules are far from being understood.[11] In the presence of nanomateriales, biomolecules may induce phase transformations, restructuring, and dissolution at the nanomaterial surface.

On the other hand, Langmuir monolayers of phospholipids, fatty acids and other amphiphiles have been widely employed as biomimetic models for studying the behavior of bioactive amphipatic molecules and the important information derived from them, constituted the very basis of our understanding of the membrane structural dynamics and response on molecular terms.[12,13] The organization of monolayer components in two dimensions makes such systems amenable for comprehensive physicochemical investigation and structural manipulation of surface properties under controlled molecular conditions.

Regarding the molecular basis of nanoparticle/biointerface interactions some important contributions have been recently made, showing the dependence on the system composition and their chemical features.[14−19]

In this work, we focused on the interaction between saturated or unsaturated lipids with relatively simple MNP by using Langmuir isotherms, the thermodynamics functions derived from them, and Brewster angle microscopy (BAM) to investigate the lateral molecular packing, miscibility, and surface topography of the film. The MNP used are functionalized by a single layer of oleic acid (OA).[20] Our results indicate they induce noticeable changes in the lipids films properties and in the surface topography of the phospholipids that are noteworthy different depending on the lipid alkyl chain saturation degree.

EXPERIMENTAL SECTION

Materials. The phospholipids 1,2-dimyristoyl-*sn*-glycero-3-phosphocholine (DMPC), 1,2-dipalmitoyl-*sn*-glycero-3-phosphocholine (DPPC), 1,2-distearoyl-*sn*-glycero-3-phosphocholine (DSPC), and 1-palmitoyl-2-oleoyl-*sn*-glycero-3-phosphocholine (POPC) were purchased from Avanti Polar Lipids (Alabaster, AL). Oleic acid (OA) used for the monolayer experiments was of the same quality as that used for the synthesis of the single-layer coated magnetic nanoparticles (MNP@OA). The purity of OA (Anedra, RA Reagent Ph. Eur) was ascertained by ^{1}H NMR and ^{13}C NMR.

All solvents and chemicals used were of the highest commercial purity available. Water was deionized by using a Milli-Q system (Millipore) 18 MΩ.cm.

Synthesis of Single-Layer Oleic Acid Coated Magnetic Nanoparticles (MNP@OA). MNP@OA were prepared by a slight modification of the two step process described by Peng et al.[20] In the first step, 1.5 g (7.5 mmol) of ferrous chloride tetrahydrate ($FeCl_2 \cdot 4H_2O$) and 4.1 g (15.2 mmol) of ferric chloride hexahydrate ($FeCl_3 \cdot 6H_2O$) were dissolved in 120 mL of deionized water in a flask at 85 °C. This solution was stirred vigorously, followed by the quickly adding of 20 mL 28% (w/w) $NH_3 \cdot H_2O$ at room temperature. The solution color changed from orange to black, leading to a black precipitate. Then 1 mL of OA (3 mmol) was dropped slowly under vigorous stirring at 80 °C in 1 h. The whole process was carried out under a N_2 atmosphere. The resulting magnetic nanoparticles coated by OA were well dispersed in water by protection of a double layer of OA.

The second step was the extraction of the magnetite nanoparticles possessing a double layer of OA from water into an organic phase. Briefly, 50 mL of MNPs' water dispersion was mixed with 50 mL of toluene in a separating funnel. Addition of a small amount of sodium chloride resulted in the transfer of MNP@OA into the toluene phase. Finally, toluene was concentrated under reduced pressure to 20 mL and the black precipitate was washed 3 times with pure ethanol through magnetic decantation.

The MNP@OA obtained were characterized by different techniques (see below) that confirmed the presence of the magnetite core (Fe_3O_4) with an average diameter of 9.5 nm and a single−layer of OA (see Supporting Information Figures S1−S4).

Characterization of MNP@OA. The nanoparticle size and shape were determined by transmission electron microscopy (TEM) using a JEM-2100F instrument, with the microscope operating at an accelerating voltage of 200 kV. The sample was prepared by placing a small drop of nanoparticles dispersed in ethanol onto the EM copper grid and the solvent was left to evaporate.

FT-IR spectra of MNP@OA (mixed with KBr) and OA (deposited on a AgBr disc support) were measured in a Nicolet 5XC spectrophotometer.

Thermogravimetric analysis (TGA) was carried out on a PerkinElmer Pyris thermal analyzer at a heating rate of 10 °C min^{-1} under nitrogen flow over a range of 30−800 °C.

The powder diffraction pattern was obtained on a Philips PAN analytical X'pert using Cu Kα radiation beam (λ = 0.15406 nm) operated at voltage of 40 kV and current of 30 mA. Diffraction patterns were collected in the range 20−80° (2θ).

TEM images, FT-IR spectra, X-ray powder diffraction patterns, and TGA are shown in Figures S1−S4.

Preparation of Langmuir Monolayers. The films of pure lipid, pure MNP@OA, or their mixed monolayers in the desired proportions were prepared by seeding their chloroform solution at the air/water interface. Mixed monolayers were obtained as follows: chloroform solutions of each material were premixed and spread onto the water interface. After that, solvent evaporation was allowed for 20 min and the monolayer at the air/water interface was compressed at a rate of 10 mm/min at room temperature (23−25 °C). The absence of surface active impurities in the spreading solvent and aqueous subphase was routinely checked before each run as reported elsewhere.[21,22] Surface pressure was measured by a platinized-Pt sensing plate. At least three surface pressure−mean area isotherms were obtained and averaged. Reduction of the routine compression speed (10 mm/min) by half did not alter the isotherms. Reproducibility was within a maximum standard error of the mean (SEM) of 1 mN/m for the surface pressure and under 1% of the mean area. The concentration of MNP@OA solutions was estimated by using the average weight of the MNP@OA calculated on the basis of the chemical characterization described above. An operational nanoparticle weight was calculated by considering the volume of spheres with an average diameter of 9.5 nm, the specific density of Fe_3O_4 (5.2 kg/dm^3), and the number of molecules of OA on the nanoparticle surface considering a complete coverage by a single layer of OA. The average cross-sectional area occupied by one OA molecule at the particle surface was taken as 30 Å^2/molecule,[13] giving a total of about 914 molecules of OA per MNP; this amount of OA coincides with that experimentally determined by

dx.doi.org/10.1021/la500903m | Langmuir XXXX, XXX, XXX−XXX

TGA.[23] The estimated average weight of the MNP@OA was 1661 kDa.

In order to determine deviations from the ideal behavior, the experimental isotherms of the mixed monolayers were compared to the ideally mixed films. The ideally mixed isotherms were calculated according to eq 1 for a binary mixture (phospholipid/MNP@OA or phospholipid/phospholipid) or eq 2 for a ternary mixture (phospholipid/phospholipid/MNP@OA):[24]

$$A_{\text{ideal}} = [A^{\text{L1}}X^{\text{L1}} + A^{\text{MNP@OA}}X^{\text{MNP@OA}}]_{\pi} \quad (1)$$

$$A_{\text{ideal}} = [A^{\text{L1}}X^{\text{L1}} + A^{\text{L2}}X^{\text{L2}} + A^{\text{MNP@OA}}X^{\text{MNP@OA}}]_{\pi} \quad (2)$$

where A_{ideal} is the calculated area at a constant surface pressure for an ideally mixed film, A^{L1}, A^{L2}, and $A^{\text{MNP@OA}}$ are the areas defined for the pure lipid/s and nanoparticle, and X^{L1}, X^{L2}, and $X^{\text{MNP@OA}}$ are the mole fraction of the lipid/s and nanoparticle, respectively. The mole fractions of MNP@OA and lipids were calculated according to eqs 4 and 5, and the mole fraction of OA present on the MNP@OA surface was estimated by considering a quantity of 914 molecules of OA per nanoparticle; in this manner, a sample containing $X^{\text{MNP@OA}} = 0.0003$ corresponds to $X^{\text{OA}} = 0.21$.

$$X^{\text{MNP@OA}} = \frac{\text{mole}^{\text{MNP@OA}}}{\text{mole}^{\text{MNP@OA}} + \text{mole}^{\text{lipid}}} \quad (4)$$

$$X^{\text{L}} = \frac{\text{mole}^{\text{lipid}}}{\text{mole}^{\text{MNP@OA}} + \text{mole}^{\text{lipid}}} \quad (5)$$

The interfacial elastic modulus of area compressibility, reflecting variations of the film in-plane elasticity, was calculated as $K = \text{Cs}^{-1} = -A(\text{d}\pi/\text{d}A)$, where Cs is the compressibility and A is the area at each surface pressure (π) point of the isotherm.[24]

The compression−expansion free energy (ΔG) was calculated from the compression or expansion isotherms according to eq 6.[22]

$$\Delta G = \int_{\pi=2}^{\pi=21} A_{\pi}\, \text{d}\pi \quad (6)$$

The thermodynamic functions of hysteresis for the MNP@OA films were calculated as the difference between the values of expansion and those of compression, as a reference. These calculations had been made by using MNP@OA isotherms that did not experienced collapse and by taking into account values of surface pressure between 2 mN/m (which avoids the contribution of the uncertain gaseous−like phase) and 21 mN/m of the compression−expansion isotherms (prior to reaching collapse). Ideal films show no hysteresis, so $\Delta G_i^{\text{hys}} = 0$, $\Delta S_i^{\text{hys}} = 0$, $\Delta H_i^{\text{hys}} = 0$. The free energy of hysteresis ΔG^{hys}, the configuracional entropy of hysteresis ΔS^{hys} (from which the entropic contribution to the free energy of hysteresis $T\Delta S^{\text{hys}}$ can be obtained), and the enthalpy of hysteresis ΔH^{hys} are defined by eqs 7−10, respectively.[25]

$$\Delta G^{\text{hys}} = \Delta G_{\text{expansion}} - \Delta G_{\text{compression}} \quad (7)$$

$$\left[\Delta S_{\pi}^{\text{hys}} = R \ln \frac{A_{\text{expansion}}}{A_{\text{compression}}}\right]_{\pi,X} \quad (8)$$

$$\Delta S^{\text{hys}} = \sum_{\pi} \Delta S_{\pi}^{\text{hys}} \quad (9)$$

$$\Delta H^{\text{hys}} = \Delta G^{\text{hys}} + T\Delta S^{\text{hys}} \quad (10)$$

Characterization of the Surface Topography. The compression and decompression isotherms were carried out in KSV Minitrough equipment (KSV, Helsinski, Finland). Brewster angle microscopy (BAM) images were obtained with an autonulling EP^3-BAM (Nanofilm Technologie GmbH, Göttingen, Germany) instrument using a 20× objective.[22,26] Images were captured with a cooled charge-coupled device (CCD) camera with a speed of 25 Hz. The wavelength of the laser beam was 532 nm and the angle of incidence was set at 53.1°. The surface pressure was measured with a KSV Minitrough mounted under the microscope. In BAM, the intensity of the reflected light represents an operational "optical thickness" that is proportional to the thickness (d) and refractive index (n) of the film.[22,26]

RESULTS AND DISCUSSION

Langmuir Monolayers of Single Magnetic Nanoparticles and Lipids. *a. Langmuir Monolayers of MNP@OA.* The surface pressure−area (π−A) compression and decompression isotherms and the compressional modulus (K) of MNP@OA are shown in Figure 1. MNP@OA form

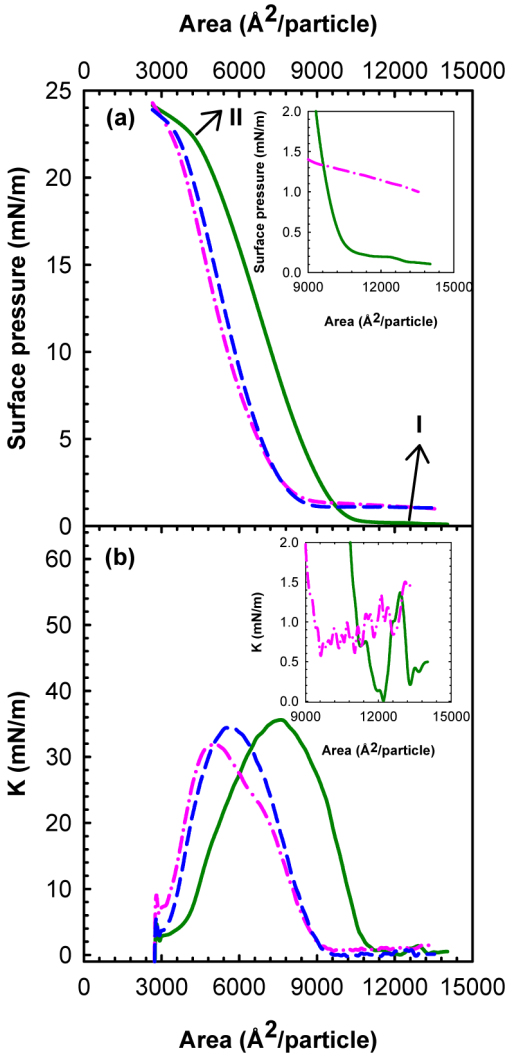

Figure 1. (a) Variation of surface pressure (inset: zoom in of the π−A isotherm region under 2 mN/m) and (b) compressional modulus of MNP@OA with the average area at the air/water interface. First compression (solid line), first decompression (dashed−dotted line), second compression (dashed line). Arrows I and II indicated the proposed organization shown in Scheme 1b.

stable monolayers at the air/water interface under successive compression−decompression cycles. At the beginning of the first compression, the pressure remains close to zero and then increases; the area obtained at the lift-off for the first compression is 13 260 Å^2/particle, while the sectional area calculated from the theoretical nanoparticles average diameter (13 nm, Scheme 1) is 13 273 Å^2/particle. However, in the

dx.doi.org/10.1021/la500903m | Langmuir XXXX, XXX, XXX−XXX

Scheme 1. (a) MNP@OA Dimensions and (b) Suggested Structures Adopted by MNP@OA at the Air/Water Interface[a]

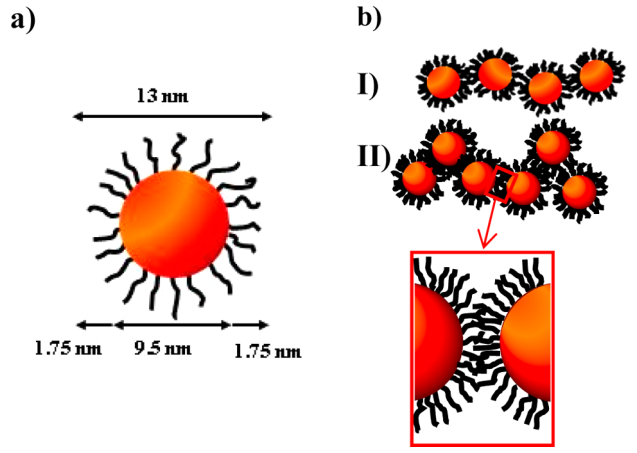

[a]MNP@OA diameter = 13 nm, magnetite core diameter = 9.5 nm, OA length = 1.75 nm. The theoretical area of MNP@OA was calculated taking into account a diameter of 13 nm obtained by considering the magnetite core diameter measured by TEM (9.5 nm) and the length of one single layer of OA covering the nanoparticle surface (1.75 nm × 2).[28] (I) Suggested structures at lift-off (I) and (II) near collapse during the first compression.

MNP@OA film, there is void space, and thus, the area obtained at the lift-off might reflect a self-organization of the nanoparticles with interdigitated OA chains and/or moderated displacements from the interfacial plane (Scheme 1, entry bI).

The limiting MNP@OA area (A_o) obtained by extrapolating the linear part of the isotherm at zero surface pressure (used to deduce the mean nanoparticle area that would be covered at zero pressure) is A_o = 9241 Å^2/particle, while at the collapse the average area is A_c = 5147 Å^2/particle at a surface pressure equal to π_c = 21.8 mN/m. The areas obtained for A_o and A_c are considerably smaller than those expected for a nanoparticle (almost 2.6 times reduction in area at collapse 13 260/5147 = ca. 2.6), suggesting a significantly degree of interdigitation of the OA chains and/or displacements from the interfacial plane as was reported before[27] (Scheme 1, entry bII).

In addition, by inspecting the 0−2 mN/m region of the first compression and the corresponding compressional modulus (K), a reproducible transition from the gaseous phase to a less compressible phase is observed indicating reorganizations and interactions among the particles in the surface (insets Figure 1). This coincides with a surface structural change from moderately reflective wire−like structures to featureless, but highly reflective, aggregates that are clearly observed by BAM when the film is compressed from the gaseous to a less compressible state (Figure 2).

The film formed by spreading of MNP@OA is stable under successive compression−decompression cycles. Furthermore, in the consecutive cycles similar limiting particle areas and collapse pressures are reached indicating that a negligible amount of particles are lost from the film into the subphase. However, the variation of the interparticle packing, and reflectance (see below) with the surface pressure are different depending on whether the particles had previously undergone compression at the interface or not. The second compression isotherm of the MNP@OA film, after having experienced a first expansion to 0 mN/m, shows that the particles are initially more closely packed as shown by the lift−off of the isotherm being left−shifted to smaller mean particles areas (Figure 1a). Furthermore, after having experienced the first compression the nanoparticle film does not return to zero surface pressure in the gas phase (Figure 1). This could be due to the adhesion of the nanoparticles to the Pt Wilhelmy plate or by the acquisition of a more ordered state after the first compression. In order to clear this point, the Pt Wilhelmy plate was thoroughly cleaned after the film was compressed and expanded, and placed again in the Wilhelmy balance. The new surface pressure remained invariant, which indicates the presence of a state with certain degree of organization. Although the isotherms exhibited hysteresis under expansion (possibly because reversible interdigitation of the OA is not complete or due to surface dislocations of the MNP@OA from the interfacial plane) the monolayers could remain stable over several hours.

Hysteresis was also studied in other nanoparticles films at the air/water interface showing to be dependent on surface functionalization of the nanoparticles among other factors.[29,30] Möhwald et al. reported the hysteresis of magnetite nanoparticles capped with catechol−terminated random copolymers of 2-(2-methoxyethoxy) ethyl methacrylate and oligo(ethylene glycol) methacrylate. During compression−expansion cycles of these nanoparticles layers, above a critical pressure, a pronounced hysteresis to smaller areas was observed. Contrary, no hysteresis of the compression−expansion isotherms results when the film is compressed below the critical pressure.[29] In our study, MNP@OA films present hysteresis either if the compression−expansion cycles are performed above or below the critical pressure.

For MNP@OA the compression free energy amounts to an average of about 73, 59, 65, and 52 kcal/mol for the first compression and decompression and second compression and decompression, respectively; from these values we can deduce that the compression work for the first compression is 10% higher than for the second compression. This result indicates that during the first compression more work is required to organize the MNP@OA film, and once the film has reached a certain degree of organization this is retained as shown by the diminished release of energy under expansion and decreased free energy of compression during the second compression.

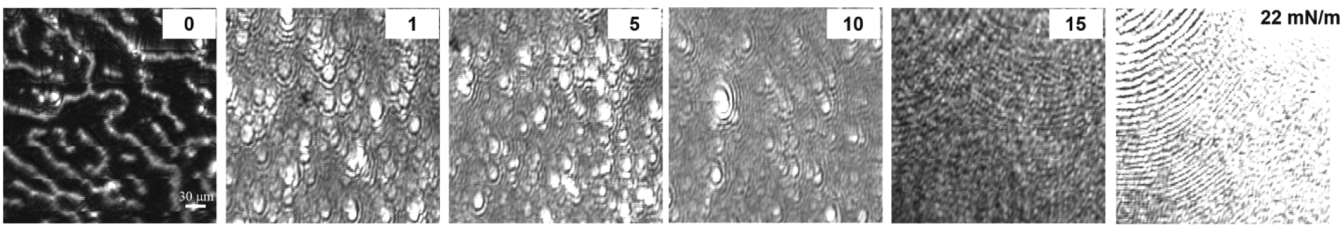

Figure 2. BAM images showing the lateral topography of MNP@OA at the air/water interface at the surface pressures indicated. Scale bar 30 μm.

dx.doi.org/10.1021/la500903m | *Langmuir* XXXX, XXX, XXX−XXX

The thermodynamic functions of hysteresis (eqs 7−10, Experimental Section), derived from the difference between the behaviors under expansion with respect to compression were calculated for the first compression−expansion cycle of the MNP@OA film.

A large negative value of ΔG^{hys} (−13.7 kcal/mol) indicates the retention of a considerable amount of free energy during the first compression which implies that the behavior of the MNP@OA film depends on the history of the system and indicates capacity of the film to store organizational information. The energy stored as free energy of hysteresis during the first compression represents the balance of enthalpic and entropic contributions. For MNP@OA film it is noticeable that the main contribution to the free energy of hysteresis arises from favorable enthalpy (ΔH^{hys} = −15.6 kcal/mol) with a smaller entropically unfavorable contribution from the term $T\Delta S^{hys}$ (−1.94 kcal/mol) due to the increased molecular ordering acquired under compression.

The formation of the MNP@OA film was also followed by BAM to inspect the lateral topography of the film spread at the air/water interface. Figure 2 shows the BAM images obtained during the first compression. The BAM experiments are in line with the phase changes observed in the isotherm. At zero pressure, before reaching the lift-off pressure, MNP@OA are organized in the film as wirelike structures. Above the lift-off, and while the surface pressure is increased, complete coverage of the surface is achieved and bright regions are apparent at the surface indicating an increase in the optical thickness of the film during compression. Due to the reflectivity increase during compression it was necessary to change the BAM polarizer position (with respect to the initial BAM set up) in order to avoid bleaching the images. It can be noted in Figure 2 that some areas appear brighter than others. Given the principles of BAM, the variation of optical thickness may reflect changes in the monolayer thickness, of the refraction index, or variations of both. BAM images at surface pressures above 15 mN/m also show reproducible long-range-order structures of well organized fingerprint interference patterns.

Considering the information extracted from the π−A isotherms and the BAM micrographs, we suggest the MNP@OA might adopt the organization proposed in Scheme 1.[27]

b. Langmuir Monolayers of Lipids. The lipids used in this work were DMPC, DPPC, DSPC, POPC, and OA for which the thermodynamics properties have been widely investigated.[13,31−33] The features of π−A isotherms obtained are in agreement with previous literature reports. These lipids cover a wide range of phase states and degree of hydrocarbon chain saturation degree. The pure lipids isotherms (Figure S5) as well as the BAM images obtained are shown in the next sections and in the Supporting Information.

Mixed Lipid/MNP@OA Langmuir Monolayers. In order to investigate the effects of MNP@OA in the phospholipid monolayers a solution containing MNP@OA and lipid(s) was spread at the air/water interface. In all experiments, the mole fraction of MNP@OA used was $X^{MNP@OA}$ = 0.0003.

a. Saturated−Chain Phospholipids: DMPC, DPPC, and DSPC. The saturated choline phospholipids selected for this study contain acyl chains of varying length, and consequently adopt different phases at the air/water interface at room temperature: DMPC (14 carbons in each of the saturated acyl chains) exists in a liquid-expanded (LE) state over the entire compression isotherm, DPPC (16 carbons saturated acyl chains) exhibits a transition between a liquid-expanded (LE) and liquid-condensed (LC) state, while DSPC (18 carbons saturated acyl chains) forms fully condensed monolayers.

Figure 3 shows the π−A isotherms of pure saturated phospholipids (DMPC, DPPC, and DSPC), of pure MNP@OA, and of the experimental and ideally mixed monolayer containing the lipid and the nanoparticles with a mole fraction of $X^{MNP@OA}$ = 0.0003.

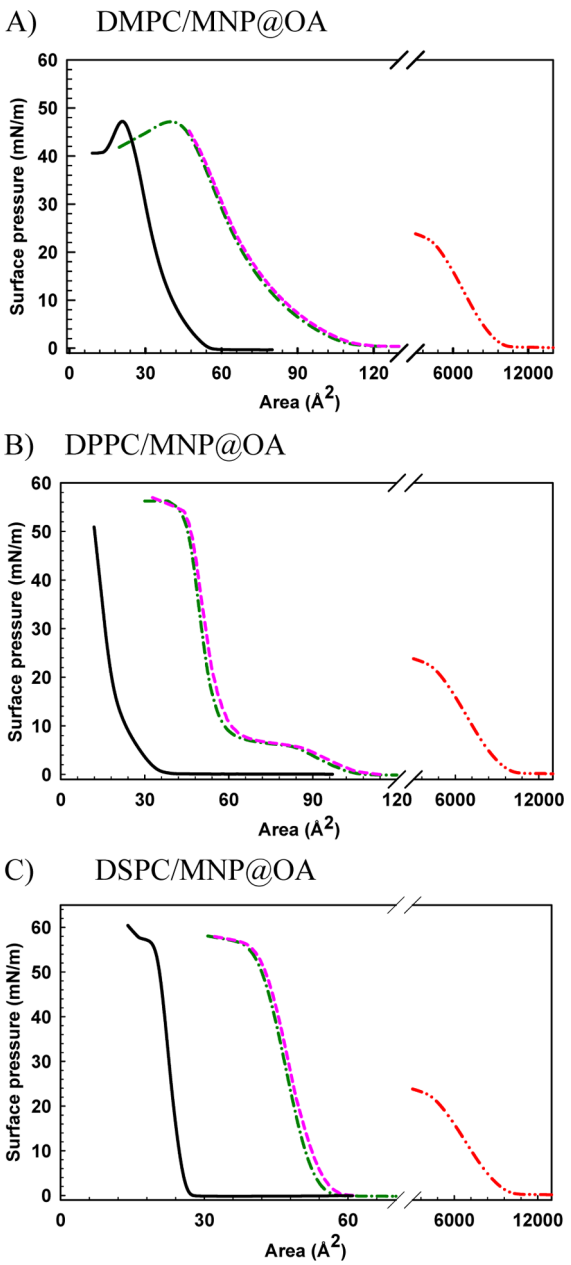

Figure 3. π−A isotherm for (A) DMPC, (B) DPPC, and (C) DSPC mixed with MNP@OA spread at the air/water interface. Pure phospholipid (dash-dot), pure MNP@OA (dash-dot-dot), experimental (solid), and ideal (dash) mixed monolayer with $X^{MNP@OA}$ = 0.0003.

It can be seen that with all saturated phospholipids the presence of the MNP@OA shifts the isotherms to much smaller molecular areas, not only compared to those of the ideally mixed film but also than those expected even for a pure phospholipid (see below) suggesting that part of the material may be lost from the interfacial plane. Besides, the presence of the nanoparticles causes phase condensation of the saturated

dx.doi.org/10.1021/la500903m | Langmuir XXXX, XXX, XXX−XXX

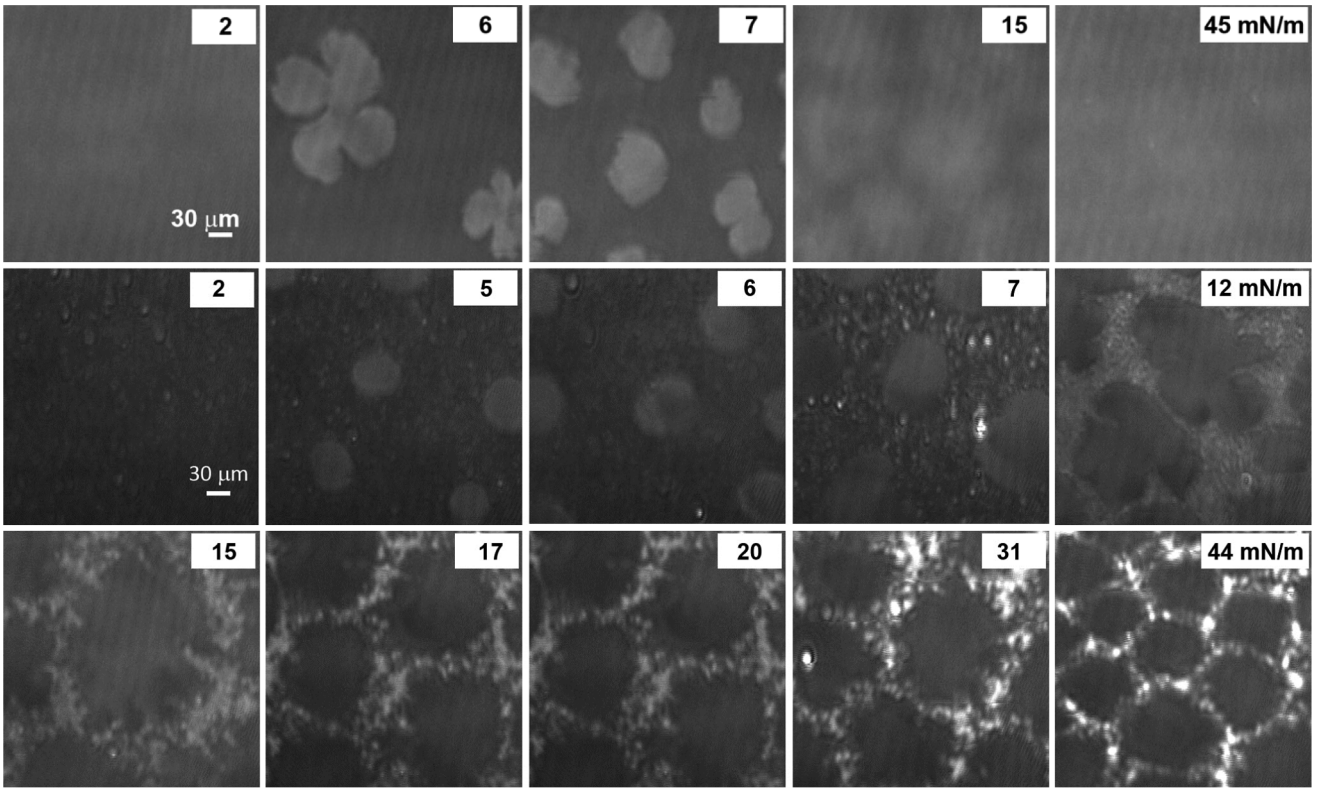

Figure 4. BAM images of pure DPPC (upper panel) and the mixture DPPC/MNP@OA (lower panels) spread on pure water at different surface pressure. Scale bar 30 μm.

lipids indicating that the incorporation of MNP@OA in the films modifies the molecular properties and phase state of the lipids as shown by the comparison with the calculated isotherms assuming ideal mixing (see Figure 3).

The BAM images, which show the mesoscale organization of the film, enable us to visualize the presence of nanoparticles immersed in the lipid matrix at the film surface even though the areas obtained for the mixed film are smaller than those expected. This suggest that the loss of MNP@OA and/or phospholipids from the surface is only partial (Figure 4 and Figures S6 and S7).

The compressional modulus (K) of the mixtures saturated phospholipids/MNP@OA has been analyzed (Figure S8). For DPPC/MNP@OA films kinks and inflections are observed at surface pressures near 1 mN/m, 4 and 24 mN/m that are in near coincidence with the disappearance of the gas phase of MNP@OA film, the beginning of the LE−LC phase coexistence in DPPC, and the collapse pressure of MNP@OA. The same trend in K is observed for the mixture DMPC/MNP@OA which also shows reorganizations at pressures near the ending of the MNP@OA gaseous phase. On the other hand, the K plot for DSPC/MNP@OA only shows an inflection near the collapse pressure of the MNP@OA, at about 25 mN/m, with absence of the reorganization at low surfaces pressures associated with the loss of the MNP@OA gas phase (contrary to that observed with the phospholipids that possess LE phases, see below). The appearance of phase transition points similar to those of the pure compounds in the mixed monolayers suggests the existence of a pure phospholipid phase in the mixed monolayer. That is, the two components may not be completely miscible in the mixed film.

Pure DPPC exhibits a defined cooperative phase transition from the LE to the LC state at about 7 mN/m.[24] The presence of MNP@OA leads to a much reduced cooperativity (though still noticeable) of the DPPC liquid expanded−condensed transition region and induces condensation, with a large shift of the isotherm to much smaller mean areas than those occupied by DPPC at all surface pressures. As mentioned above, the BAM experiments indicate the presence of the MNP@OA in the film showing that they are not completely squeezed out of the monolayer but remain at the surface segregated from the LC DPPC domains, Figure 4.

Figure 4 compares the topography observed by BAM for pure DPPC and the mixture DPPC/MNP@OA. It can be seen that the nanoparticles significantly modify the surface topography of DPPC along the whole isotherm even if they constitute only a very small mole fraction of the mixture. At low surface pressures (0−3 mN/m), the nanoparticles are observed as bright spots on the surface (at such surface pressures pure DPPC shows a homogeneous topography corresponding to the LE phase).

With the increase of surface pressure the formation of LC domains of DPPC is observed but the presence of MNP@OA induces the loss of their typical triskelion shape. Also, it can be seen that the nanoparticles preferentially partition into the LE phase of DPPC. Further increases of surface pressure lead to the increase of the amount of LC phase of DPPC as expected, but the presence of MNP@OA in the LE phase of the film impairs the coalescence of the LC domains as it occurs with pure DPPC. The BAM images show phase segregation between the LE phase containing the MNP@OA and the LC phase of DPPC, with the establishment of a hexagonal lattice of LC domains of DPPC surrounded by a net of MNP@OA (lower

dx.doi.org/10.1021/la500903m | *Langmuir* XXXX, XXX, XXX−XXX

panel). This hexagonal lattice shows long-range order along the entire surface.

Incidentally, the spacing among condensed domains at close packing is in the order of about 10 μm which roughly coincides with the periodicity of some fingering patterns observed in MNP@OA films (see Figure 2).

To ascertain whether the observed effects are specifically due to the presence of MNP@OA in the DPPC film or only to the oleate chains covering the nanoparticles, we studied the mixture of DPPC/OA. The proportion of OA used in the mixed monolayer was equal to that provided by the MNP@OA (a sample with a mole fraction $X^{MNP@OA} = 0.0003$ corresponds to a mole fraction of $X^{OA} = 0.21$), the isotherms and BAM images are shown in Figures S9 and S10. Neither the $\pi-A$ isotherm nor the BAM images of DPPC/OA exhibit the features observed in the mixture DPPC/MNP@OA, which leads us to conclude that the observed behavior is specifically due to the presence of MNP@OA in the DPPC film.

In order to determine if these interesting topographic features also arise when MNP@OA are offered to another surface with LE/LC phase coexistence, we studied the mixture of DMPC/DSPC alone and in the presence of MNP@OA. DMPC is a phospholipid that shows a LE phase, and DSPC exhibits a condensed phase over the entire isotherm; when mixed, they show coexistence of discrete domains of a long-range ordered condensed phase dispersed in a continuous, disordered, LE phase.[34] The isotherms and BAM images for these mixtures are shown in Figures S11 and S12. As can be seen from the isotherm and BAM micrographs the behavior observed for the mixture DMPC/DSPC with MNP@OA is similar to that observed with DPPC. The presence of MNP@OA in the DMPC/DSPC film also induces a shift of the isotherm to smaller areas than those that would be occupied by a phospholipid molecule; similarly, the nanoparticles are preferentially partitioned in the LE phase, comparable to what was observed with DPPC, and form a lattice that holds the condensed domains separated impeding their coalescence (Figure S12).

In the case of the mixtures DMPC/MNP@OA and DSPC/MNP@OA, the $\pi-A$ isotherms also show shifts to smaller areas than that of a single phospholipid molecule in condensed state. Regarding the topography, the MNP@OA are observed in the film surface with a distribution similar to that acquired when they are alone. In Figure S6, it can be seen the characteristic wirelike distribution of the MNP@OA immersed in the DMPC film in the gaseous phase (0 mN/m); this was not observed with DSPC.

b. Unsaturated–Chain Lipids: POPC and Oleic Acid. The unsaturated phosphatydilcholine selected for this study was POPC in which one of the acyl chain is OA and the other is a saturated one; POPC has a LE phase state along the whole isotherm. Also we studied the interaction of MNP@OA with OA. The general trend observed for the interaction of MNP@OA with these unsaturated lipids is completely different than that observed with the saturated ones.

Figures 5 compares the $\pi-A$ isotherms of pure POPC (or OA) and pure MNP@OA, with the experimental and ideally mixed monolayers containing the lipid and a molar fraction of MNP@OA of $X^{MNP@OA} = 0.0003$. Noteworthy, it was found that with the unsaturated lipids the presence of the MNP@OA shifts the isotherms to molecular areas that are expanded but remain between those of the pure components. Also, the

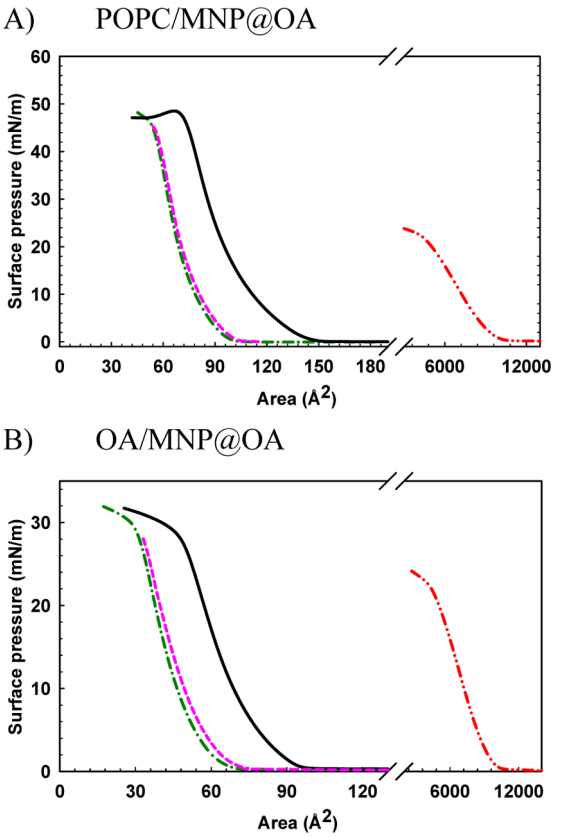

Figure 5. $\pi-A$ isotherm for (A) POPC and (B) OA mixed with MNP@OA spread at the air/water interface. Pure lipid (dash-dot), pure MNP@OA (dash-dot-dot), experimental (solid), and ideal (dash) mixed monolayer with $X^{MNP@OA} = 0.0003$.

average area occupied by the mixture is larger than that calculated assuming ideal interactions between the components.

Figure 6 shows the lateral topography observed by BAM for POPC and POPC/MNP@OA, and Figure S13 the topography of OA and OA/MNP@OA. Either mixture with POPC or OA shows the presence of MNP@OA at the film surface, although the MNP@OA are less evident than with the saturated phospholipids; this probably indicates a better mixing of the particles with the unsaturated lipids, with less optical dislocation (thickness, interfacial location and/or variation of the refraction index) in the interfacial plane.

CONCLUSIONS

In this work, we have been able to form and characterize MNP@OA films at the air/water interface as well as their mixed films with saturated and unsaturated lipids.

The MNP@OA films are stable under successive compression–decompression cycles. The area obtained at collapse is smaller than that expected for a single nanoparticle suggesting the nanoparticles may self-organize with interdigitated OA chains and/or become displaced from the interfacial plane. From the compression work, we calculated that 10% more energy is required for the first compression compared to the second one to closely pack the particles indicating that more energy is involved to first organize the MNP@OA film. After the film has acquired a certain degree of organization under compression, the latter is retained as clearly evidenced by the diminished release of energy under expansion and the decreased free energy of compression during the second

dx.doi.org/10.1021/la500903m | *Langmuir* XXXX, XXX, XXX–XXX

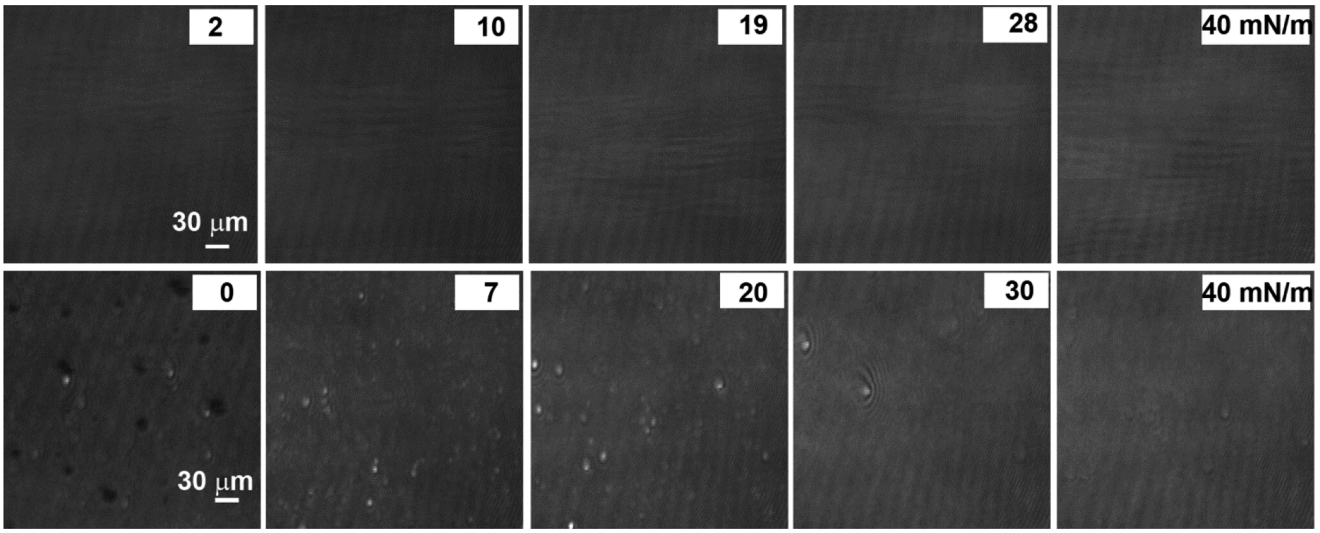

Figure 6. BAM images of pure POPC (upper panel) and the mixture of POPC/MNP@OA (lower panel) spread on pure water at different surface pressure. Scale bar 30 μm.

compression. The large negative value obtained for ΔG^{hys}, mostly contributed by favorable enthalpic contributions, indicates the capacity of the MNP@OA films to store energy in the form of organizational information.

A relevant topic to be considered in nanomedicine and drug delivery is nanoparticle toxicity. The main variables that determine nanoparticle in vivo biocompatibility are size, zeta potential (surface charge), and dispersibility (particularly the effect of hydrophobicity). Low toxicity is favored by a large size, relatively hydrophobic or poorly water dispersed particles, which are rapidly and safely removed by the reticuloendothelial system (RES).[4,6] The MNP@OA used in this work match quite well with the low toxicity characteristic described above. Nevertheless, they notably modify the properties of phospholipids monolayers depending on the acyl chain type of the latter.

Regarding the interaction of phospholipids with MNP@OA, a selective interaction among the particles with saturated and unsaturated phospholipids was found which is reflected by the isotherms as well as by the topography of the films. The interaction of these magnetic nanoparticles with saturated lipids cause a noticeable reduction of the film area, while the interaction with unsaturated lipids occur with area expansion, compared to ideally mixed isotherms. Moreover, when there is an isobaric coexistence of LE−LC phases, the nanoparticles preferably partition to the LE phase, thus impeding the coalescence of condensed domains under increasing surface pressure. All these findings show a markedly sensitive composition-dependent regulation of the surface−nanoparticle interactions with biomembrane phospholipids. The results point out the biophysical relevance of understanding nanoparticle functionalization in relation to its interactions in biointerfaces constituted by defined types of biomolecules. This is important for controlling the nanoparticle capacity to disperse in biomolecular surfaces and for the spontaneous acquisition of self-assembled interfaces with purposely designed surface topography, elasticity, lateral packing, and phase domain structuring.

■ ASSOCIATED CONTENT

Ⓢ Supporting Information

Characterization of MNP@OA (S1−S4) and complementary isotherms and BAM images (S5−S15). This material is available free of charge via the Internet at http://pubs.acs.org.

■ AUTHOR INFORMATION

Corresponding Author

*Tel.: +54 351 5353867. Fax: +54 351 4334074. E-mail: rvico@fcq.unc.edu.ar.

Notes

The authors declare no competing financial interest.

■ ACKNOWLEDGMENTS

This work was supported by MINCyT−DST Project SA 10/01 Argentina−South Africa, SECyT−UNC, CONICET, FONCYT. T.J.M. is a doctoral student at Rhodes University. A.E.L. is a doctoral fellow of CONICET. R.W.M.K is a Professor at Rhodes University, and B.M., A.M.G., and R.V.V. are Career Investigator of CONICET.

■ REFERENCES

(1) Kim, S. T.; Saha, K.; Kim, C.; Rotello, V. M. The Role of Surface Functionality in Determining Nanoparticle Cytotoxicity. *Acc. Chem. Res.* **2013**, *46*, 681−691.

(2) Canton, I.; Battaglia, G. Endocytosis at the Nanoscale. *Chem. Soc. Rev.* **2012**, *41*, 2718−2739.

(3) Cui, M.; Emrick, T.; Russell, T. P. Stabilizing Liquid Drops in Nonequilibrium Shapes by the Interfacial Jamming of Nanoparticles. *Science* **2013**, *342*, 460−463.

(4) Nel, A. E.; Mädler, L.; Velegol, D.; Xia, T.; Hoek, E. M. V; Somasundaran, P.; Klaessig, F.; Castranova, V.; Thompson, M. Understanding Biophysicochemical Interactions at the Nano-bio Interface. *Nat. Mater.* **2009**, *8*, 543−557.

(5) Mahmoudi, M.; Hofmann, H.; Rothen-Rutishauser, B.; Petri-Fink, A. Assessing the in Vitro and in Vivo Toxicity of Superparamagnetic Iron Oxide Nanoparticles. *Chem. Rev.* **2012**, *112*, 2323−2338.

(6) Zhu, M.; Nie, G.; Meng, H.; Xia, T.; Nel, A.; Zhao, Y. Physicochemical Properties Determine Nanomaterial Cellular Uptake, Transport, and Fate. *Acc. Chem. Res.* **2013**, *46*, 622−631.

(7) Nangia, S.; Sureshkumar, R. Effects of Nanoparticle Charge and Shape Anisotropy on Translocation Through Cell Membranes. *Langmuir* **2012**, *28*, 17666−17671.
(8) Cho, E. C.; Xie, J.; Wurm, P. a; Xia, Y. Understanding the Role of Surface Charges in Cellular Adsorption Versus Internalization by Selectively Removing Gold Nanoparticles on the Cell Surface with a I2/KI Etchant. *Nano Lett.* **2009**, *9*, 1080−1084.
(9) Lu, A.-H.; Salabas, E. L.; Schüth, F. Magnetic Nanoparticles: Synthesis, Protection, Functionalization, and Application. *Angew. Chem., Int. Ed. Engl.* **2007**, *46*, 1222−1244.
(10) Koo, H.; Huh, M. S.; Sun, I.-C.; Yuk, S. H.; Choi, K.; Kim, K.; Kwon, I. C. In Vivo Targeted Delivery of Nanoparticles for Theranosis. *Acc. Chem. Res.* **2011**, *44*, 1018−1028.
(11) Reddy, L. H.; Arias, J. L.; Nicolas, J.; Couvreur, P. Magnetic Nanoparticles: Design and Characterization, Toxicity and Biocompatibility, Pharmaceutical and Biomedical Applications. *Chem. Rev.* **2012**, *112*, 5818−5878.
(12) Brockman, H. L. Lipid Monolayers: Why Use Half a Membrane to Characterize Protein-membrane Interactions? *Curr. Opin. Struct. Biol.* **1999**, *9*, 438−443.
(13) Maggio, B.; Lucy, J. A. Studies on Mixed Monolayers of Phospholipids and Fusogenic Lipids. *Biochem. J.* **1975**, *149*, 597−608.
(14) Guzmán, E.; Liggieri, L.; Santini, E.; Ferrari, M.; Ravera, F. DPPC−DOPC Langmuir Monolayers Modified by Hydrophilic Silica Nanoparticles: Phase Behaviour, Structure and Rheology. *Colloids Surf., A* **2012**, *413*, 174−183.
(15) Guzmán, E.; Liggieri, L.; Santini, E.; Ferrari, M.; Ravera, F. Effect of Hydrophilic and Hydrophobic Nanoparticles on the Surface Pressure Response of DPPC Monolayers. *J. Phys. Chem. C* **2011**, *115*, 21715−21722.
(16) Guzmán, E.; Liggieri, L.; Santini, E.; Ferrari, M.; Ravera, F. Influence of Silica Nanoparticles on Phase Behavior and Structural Properties of DPPC-Palmitic Acid Langmuir Monolayers. *Colloids Surf., A* **2012**, *413*, 280−287.
(17) Harishchandra, R. K.; Saleem, M.; Galla, H.-J. Nanoparticle Interaction with Model Lung Surfactant Monolayers. *J. R. Soc., Interface* **2010**, *7*, S15−S26.
(18) Chao, K.-P.; Bagaria, H.; Wong, M. S.; Biswal, S. L. Templating CdSe Tetrapods at the Air/water Interface with POPC Lipids. *J. Colloid Interface Sci.* **2012**, *378*, 58−63.
(19) Wang, B.; Zhang, L.; Bae, S. C.; Granick, S. Nanoparticle-induced Surface Reconstruction of Phospholipid Membranes. *Proc. Natl. Acad. Sci. U.S.A.* **2008**, *105*, 18171−18175.
(20) Sun, Y.; Ding, X.; Zheng, Z.; Cheng, X.; Hu, X.; Peng, Y. Surface Initiated ATRP in the Synthesis of Iron Oxide/polystyrene Core/shell Nanoparticles. *Eur. Polym. J.* **2007**, *43*, 762−772.
(21) Maggio, B. Favorable and Unfavorable Lateral Interactions of Ceramide, Neutral Glycosphingolipids and Gangliosides in Mixed Monolayers. *Chem. Phys. Lipids* **2004**, *132*, 209−224.
(22) Vico, R. V.; Silva, O. F.; De Rossi, R. H.; Maggio, B. Molecular Organization, Structural Orientation, and Surface Topography of Monoacylated Beta-cyclodextrins in Monolayers at the Air-aqueous Interface. *Langmuir* **2008**, *24*, 7867−7874.
(23) Yang, K.; Peng, H.; Wen, Y.; Li, N. Re-examination of Characteristic FTIR Spectrum of Secondary Layer in Bilayer Oleic Acid-coated Fe3O4 Nanoparticles. *Appl. Surf. Sci.* **2010**, *256*, 3093−3097.
(24) George, L. *Gaines Insoluble Monolayers at the Liquid-Gas Interfaces*; Willey-Interscience: New York, 1966.
(25) Borioli, G. A.; Maggio, B. Surface Thermodynamics Reveals Selective Structural Information Storage Capacity of c-Fos-phospholipid Interactions. *Langmuir* **2006**, *22*, 1775−1781.
(26) Vico, R. V.; De Rossi, R. H.; Maggio, B. PM-IRRAS Assessment of the Compression-mediated Orientation of the Nanocavity of a Monoacylated Beta-cyclodextrin in Monolayers at the Air-water Interface. *Langmuir* **2010**, *26*, 8407−8413.
(27) Ji, X.; Wang, C.; Xu, J.; Zheng, J.; Gattás-Asfura, K. M.; Leblanc, R. M. Surface Chemistry Studies of (CdSe)ZnS Quantum Dots at the Air-water Interface. *Langmuir* **2005**, *21*, 5377−5382.
(28) Pauly, M.; Pichon, B. P.; Demortière, A.; Delahaye, J.; Leuvrey, C.; Pourroy, G.; Bégin-Colin, S. Large 2D Monolayer Assemblies of Iron Oxide Nanocrystals by the Langmuir−Blodgett Technique. *Superlattices Microstruct.* **2009**, *46*, 195−204.
(29) Stefaniu, C.; Chanana, M.; Wang, D.; Novikov, D. V.; Brezesinski, G.; Möhwald, H. Langmuir and Gibbs Magnetite NP Layers at the Air/water Interface. *Langmuir* **2011**, *27*, 1192−1199.
(30) Shen, Y.-J.; Lee, Y.-L.; Yang, Y.-M. Monolayer Behavior and Langmuir−Blodgett Manipulation of CdS Quantum Dots. *J. Phys. Chem. B* **2006**, *110*, 9556−9564.
(31) Smaby, J. M.; Momsen, M. M.; Brockman, H. L.; Brown, R. E. Phosphatidylcholine Acyl Unsaturation Modulates the Decrease in Interfacial Elasticity Induced by Cholesterol. *Biophys. J.* **1997**, *73*, 1492−1505.
(32) Ha, T. H.; Kim, D. K.; Choi, M.-U.; Kim, K. Influence of Poly(ethylenimine) on the Monolayer of Oleic Acid at the Air/Water Interface. *J. Colloid Interface Sci.* **2000**, *226*, 98−104.
(33) Rolland, J. P.; Santaella, C.; Vierling, P. Molecular Packing of Highly Fluorinated Phosphatidylcholines in Monolayers. *Chem. Phys. Lipids* **1996**, *79*, 71−77.
(34) Wilke, N.; Vega Mercado, F.; Maggio, B. Rheological Properties of a Two Phase Lipid Monolayer at the Air/water Interface: Effect of the Composition of the Mixture. *Langmuir* **2010**, *26*, 11050−11059.